

Article

# Theoretical Study of a Surface Collinear Holographic Memory

Soki Hirayama <sup>1</sup>, Ryushi Fujimura <sup>2</sup>, Shinsuke Umegaki <sup>1</sup>, Yoshito Y. Tanaka <sup>1</sup> and Tsutomu Shimura <sup>1,\*</sup>

<sup>1</sup> Institute of Industrial Science, The University of Tokyo, Tokyo 153-5805, Japan;

skhrym@iis.u-tokyo.ac.jp (S.H.); umegaki@iis.u-tokyo.ac.jp (S.U.); yoshito@iis.u-tokyo.ac.jp (Y.Y.T.)

<sup>2</sup> Division of Engineering and Agriculture, Utsunomiya University, Tochigi 321-8585, Japan; fujimura\_r@cc.utsunomiya-u.ac.jp

\* Correspondence: shimura@iis.u-tokyo.ac.jp

Received: 15 May 2019; Accepted: 11 June 2019; Published: 19 June 2019



**Abstract:** Holographic memory is currently attracting attention as a data storage system capable of achieving a data transfer rate of about  $10^5$ – $10^6$  times that of an optical disc such as Blu-ray disc. In conventional holographic memory, data is generally recorded by optical writing using volume holograms. However, a volume hologram has the problem not only that it is required to have high mechanical accuracy of a system and low coefficient of thermal expansion of a recording medium, because reconstruction tolerance is extremely low, but also that duplicating time efficiency is poor because whole data cannot be recorded at once. In this paper we proposed surface holographic memory that achieved a high data transfer rate, stable readout performance, and collective duplication by expressing holograms with fine surface asperity. Furthermore, the theoretical formulas of recording and reconstruction processes in the proposed system were derived and the reconstruction characteristics of the hologram were evaluated by numerical simulation. As a result, the proposed method generated reconstructed image readout with sufficient signal for a single page recording. However, the reconstructed image had noise, which was particular to a surface holographic memory.

**Keywords:** holographic memory; collinear; Raman–Nath diffraction

## 1. Introduction

In recent years, the amount of information exchanged is increasing explosively as the demand for big data increases with the development of artificial intelligence (AI) technology and the densification of information advances with the advent of high-resolution equipment. Most of such data is called “Cold Data”, which is not accessed frequently but needs to be stored for a long time. These data correspond to not only big data used in AI technology but also digital data of historical materials, video recording data of surveillance cameras and television stations, logistics records and medical records. The mainstream of current data storage systems is hard disk drive (HDD), which is a magnetic recording. However, considering that HDD requires a cooling system for constant running and needs regular backup, the total cost of ownership for maintaining data for a long time can be enormous.

Therefore, in cases of recording and maintaining cold data, it has become necessary to shift to a data storage system that has a lower total cost of ownership than HDD and can be stored for a long time. Optical disks are more suitable for recording and maintaining cold data than HDD because they consume less power to maintain data and can store data stably for a long time by recording data depending on fine and uneven surface shape. However, since the Blu-ray disc, a typical optical disc, has a bit-by-bit system, the data transfer rate is limited, and it has been regarded as too slow to transfer large-capacity data in recent years. In order to improve the data transfer rate, a parallel

reading method using a multi-head has been proposed, but while the system becomes complicated the data transfer rate is about two to four times. Therefore, it has not been able to keep up with the demand for high-speed reading and high-speed duplication of ever-growing large-capacity data.

With such a background, holographic memory is currently attracting attention [1–3] as an optical memory that is expected to break through the limits of data transfer rates and achieve about  $10^5\sim 10^6$  times the transfer rate by a method that is fundamentally different from conventional optical disks. Holographic memory is an optical storage system proposed by P. J. van Heerden in 1963 [4] based on the principle of holography proposed by D. Gabor [5]. It is possible to dramatically improve the data transfer rate by collectively recording and reconstructing two-dimensional data.

In conventional holographic memories, interference fringes written in a volume hologram are generally recorded three-dimensionally. However, in the case of volume hologram and while high-density multiple recording is possible, the system requires high mechanical control accuracy for identifying each recorded data page and low coefficient of thermal expansion of a recording medium to prevent the interference pattern recorded from changing. This is because reconstruction tolerance of volume holograms is much lower, due to Bragg diffraction, than that of surface holograms. Moreover, recording and duplicating cannot be performed collectively, which causes a problem of time inefficiency.

In this paper, we propose surface holographic memory that expresses a hologram by fine surface asperity processing, instead of recording a hologram by optical writing as in the conventional method.

This paper is organized as follows; Chapter 2 outlines the surface holographic memory proposed in this paper. Chapter 3 shows the principle of recording and reconstruction of the proposed method. Chapter 4 evaluates the reconstruction characteristics of the hologram in the proposed system by numerical calculation and shows the results. Chapter 5 considers the noise specific to a surface holographic memory, and finally Chapter 6 gives the conclusions of this paper.

## 2. Surface Collinear Holographic Memory

The optical system of the surface collinear holographic memory proposed in this paper is shown in Figure 1. Figure 1a shows the optical system assumed to be designed in the case of reconstruction, and Figure 1b shows the optical system assumed for calculation in the case of hologram design. One of the most important features of the proposed method is that the optical system, as shown in Figure 1b, is not actually set up because the hologram is designed directly instead of being recorded by light. As shown in Figure 1a,b, the wavelength is  $\lambda$ , the focal length of the lens is  $f$ , and the optical system is a  $4f$  system in the case of reconstruction, and a  $2f$  system in case of hologram designing. A phase-only surface hologram with an arbitrary step structure is disposed on the hologram plane. In the proposed method, the optical system of collinear holographic memory [6,7] in which signal pattern and reference pattern are given to one light field was assumed, as shown in Figure 1b. When designing a hologram, intensity distribution of the interference pattern between the signal pattern and the reference pattern was calculated, and the phase profile of the phase-only hologram was determined so as to have a phase distribution proportional to the intensity distribution. In the reconstruction process, the same pattern as the reference pattern assumed in the designing process was displayed on a spatial light modulator (SLM) as readout light. The phase distribution of the readout light on the hologram plane propagated from the SLM plane changed due to the phase hologram and, after transmitting, the hologram was propagated as diffracted light to the reconstructed image plane.

In the case of the surface hologram, it was impossible to record multiple holograms using the Bragg condition, as in the case of a conventional volume hologram, because surface holograms have no grating thickness. Therefore, in the proposed method, a shift multiplex method [6,8] was used in which page selectivity appeared due to destructive interference of light with random phases for multiple recording.

The surface holographic memory had some interesting features that are not found in conventional volume holographic memory. The first point was that it had a feature as a hologram whose thickness

was zero in principle. Diffraction by this hologram did not follow the Bragg diffraction model but the Raman–Nath diffraction model, and did not significantly attenuate the diffracted light even under conditions other than the Bragg match condition as in the Bragg diffraction model. This meant that the reconstructed image was less likely to be degraded against the change of the hologram accompanying the expansion and contraction, that is, changes in the recorded grating. The second point was that even a hologram, which is difficult to design when actually writing with light, could be easily realized because the hologram could be designed freely. This meant that the design of the hologram was not influenced by the physical constraints when writing with light, and it was possible to design a hologram optimized to suppress the error rate more. For example, in the conventional optical recording method of collinear holographic memory, a lot of interference between pixels in the signal area and between pixels in the reference area on the SLM plane was recorded in the hologram because multiple light sources were disposed respectively in the signal area and reference area. These interference patterns did not contribute to signal reconstruction, and cause noise. On the other hand, in the case of the surface holographic memory proposed in this paper, it was possible to design a hologram freely, and it was also possible to design a hologram from which gratings unnecessary for reconstructed signal were removed.

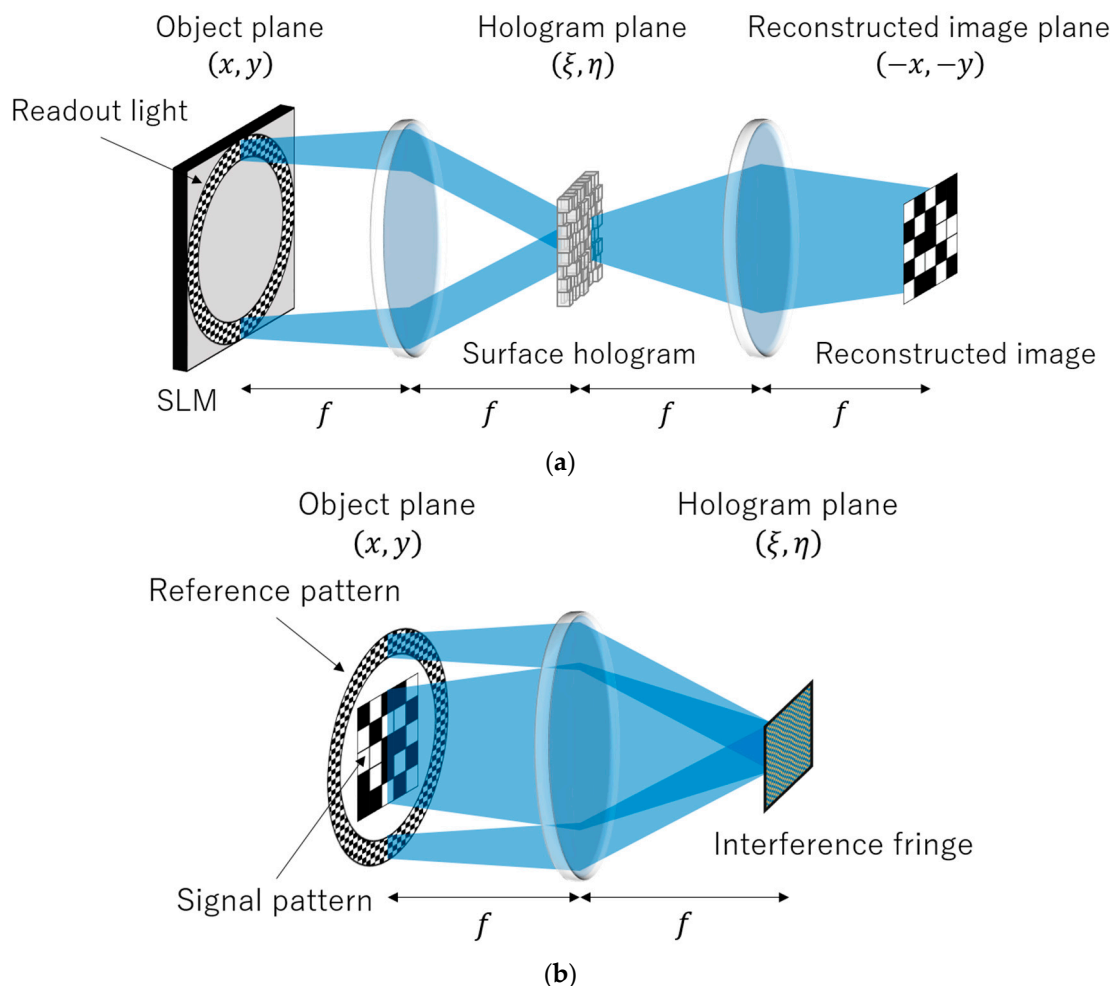


**Figure 1.** (a) Schematic of the optical system in case of reconstruction; (b) schematic of the optical system assumed for calculation in the case of hologram design.

### 3. Principle

#### 3.1. Hologram Readout

The specific design method of the hologram is described later. The complex amplitude of the reconstructed image plane, which is represented when there is a hologram having an arbitrary phase profile  $H_P(\xi, \eta)$  on the hologram plane, is described in this section. As shown in Figure 1a, the coordinates of the object plane were  $(x, y)$ , the coordinates of the hologram plane were  $(\xi, \eta)$ , and the coordinates of the reconstructed image plane were  $(-x, -y)$ . However, assuming that the readout light of the object plane is  $U_{\text{read}}(x, y)$ , the complex amplitude distribution  $U_{\text{read}}(x, y)$  of the readout light is the same as the complex amplitude distribution of the reference light assumed at the time of hologram design. At this time, the reading light  $U_{\text{read}}(\xi, \eta)$  of the hologram plane is represented by

$$U_{\text{read}}(\xi, \eta) = e^{i\pi(\frac{4f}{\lambda} - \frac{1}{2})} t_A(\xi, \eta) \mathcal{F}[U_{\text{read}}(x, y)]. \quad (1)$$

In addition,  $\mathcal{F}$  represents the two-dimensional Fourier transform from the object plane to the hologram plane, and is expressed as

$$\mathcal{F}[U(x, y)] = \frac{1}{\lambda f} \iint_{-\infty}^{\infty} U(x, y) e^{-i\frac{2\pi}{\lambda f}(\xi x + \eta y)} dx dy. \quad (2)$$

Moreover,  $t_A(\xi, \eta)$  is the transmittance of the aperture placed on the hologram plane and is expressed as

$$t_A(\xi, \eta) = \begin{cases} 1 & \text{(Inside the aperture)} \\ 0 & \text{(Outside the aperture)} \end{cases}. \quad (3)$$

An aperture placed on the hologram plane was used to limit the area of a single hologram to be recorded and to improve the recording density. Then, we considered that the light wave  $U_{\text{dif}}(\xi, \eta)$ , immediately after the readout light  $U_{\text{read}}(\xi, \eta)$  propagated to the hologram surface, had passed through the phase type hologram having an arbitrary phase profile  $H_P(\xi, \eta)$ . However, in this research, since the shift multiplexing method was used, it was necessary to consider the case of shifting the hologram on the plane. Here,  $U_{\text{dif}}(\xi, \eta)$  is represented by

$$U_{\text{dif}}(\xi, \eta) = U_{\text{read}}(\xi, \eta) e^{iH_P(\xi - \Delta\xi, \eta - \Delta\eta)}, \quad (4)$$

where  $(\Delta\xi, \Delta\eta)$  is a shift amount of the hologram. Therefore, the complex amplitude distribution  $U_{\text{dif}}(-x, -y)$  of the reconstructed image finally calculated is represented as

$$U_{\text{dif}}(-x, -y) = e^{i\pi(\frac{4f}{\lambda} - \frac{1}{2})} \mathcal{F}^{-1}[U_{\text{dif}}(\xi, \eta)]. \quad (5)$$

Here,  $\mathcal{F}^{-1}$  represents the inverse Fourier transform of the two-dimensional Fourier transform represented by Equation (2).

#### 3.2. Hologram Design

The hologram designed in this research was a phase-only hologram and was calculated based on the optical system assumed for calculation, as shown in Figure 1b. In this section, the specific design method and calculation formula of the phase profile  $H_P(\xi, \eta)$  are described. As shown in Figure 1b, the coordinates of the object plane are  $(x, y)$ , and the coordinates of the hologram plane are  $(\xi, \eta)$ . At this time, assuming that the signal light on the object plane is  $U_{\text{sig}}(x, y)$  and the reference light is  $U_{\text{ref}}(x, y)$ , the signal and the reference light on the hologram plane,  $U_{\text{sig}}(\xi, \eta)$  and  $U_{\text{ref}}(\xi, \eta)$ , are respectively represented by

$$\begin{cases} U_{\text{sig}}(\xi, \eta) = e^{i\pi(\frac{4f}{\lambda} - \frac{1}{2})} \mathcal{F}[U_{\text{sig}}(x, y)] \\ U_{\text{ref}}(\xi, \eta) = e^{i\pi(\frac{4f}{\lambda} - \frac{1}{2})} \mathcal{F}[U_{\text{ref}}(x, y)] \end{cases} \quad (6)$$

as in the reproduction. Here,  $\lambda$  is the wavelength, and  $f$  is the focal length of the lens. Therefore, the interference intensity distribution  $I(\xi, \eta)$  on the hologram plane is expressed as

$$\begin{aligned} I(\xi, \eta) &= |U_{\text{sig}}(\xi, \eta) + U_{\text{ref}}(\xi, \eta)|^2 t_A(\xi, \eta) \\ &= \left[ |U_{\text{sig}}(\xi, \eta)|^2 + |U_{\text{ref}}(\xi, \eta)|^2 + U_{\text{sig}}(\xi, \eta)U_{\text{ref}}^*(\xi, \eta) + U_{\text{sig}}^*(\xi, \eta)U_{\text{ref}}(\xi, \eta) \right] t_A(\xi, \eta). \end{aligned} \quad (7)$$

Here,  $*$  is a symbol representing a complex conjugate. The first term and the second term of Equation (7) represent interference fringes between signal light points and between reference light points respectively. The third term is a term for reconstructing the signal light and the fourth term is a term that causes a conjugate image. It should be noted that one signal light point can interfere with another signal light point and one reference light point can also interfere with another reference light point because the signal light  $U_{\text{sig}}(x, y)$  and the reference light  $U_{\text{ref}}(x, y)$  can be regarded as a group of mutually coherent light sources in the collinear method. In fact, in the intensity distribution of the interference fringes expressed by Equation (7), the diffracted light from each grating represented by the first and second terms caused noise sources that did not correctly reconstruct the recorded signal light. The intensity distribution of the interference fringes  $I(\xi, \eta)$  was equal to that on the hologram plane when the signal light pattern and reference light pattern were set by using SLM as the recording process of the conventional collinear holographic memory. When this interference pattern is applied to a phase-only hologram, its phase profile  $H_p(\xi, \eta)$  is expressed as

$$\begin{aligned} H_p(\xi, \eta) &= C_p I(\xi, \eta) \\ &= C_p \left[ |U_{\text{sig}}(\xi, \eta)|^2 + |U_{\text{ref}}(\xi, \eta)|^2 + U_{\text{sig}}(\xi, \eta)U_{\text{ref}}^*(\xi, \eta) + U_{\text{sig}}^*(\xi, \eta)U_{\text{ref}}(\xi, \eta) \right] t_A(\xi, \eta), \end{aligned} \quad (8)$$

where  $C_p$  is a phase coefficient, which does not depend on the coordinates of the hologram plane  $(\xi, \eta)$ . In the surface holographic memory proposed in this paper a hologram is not recorded by writing with light but is converted by a desired phase profile into fine surface asperity and recorded directly. Therefore, unnecessary interference fringes can be removed by directly creating a surface hologram from a phase profile not including terms corresponding to unnecessary interference fringes. Namely, the phase profile  $H'_p(\xi, \eta)$  actually designed can be represented as

$$H'_p(\xi, \eta) = C'_p \left[ U_{\text{sig}}(\xi, \eta)U_{\text{ref}}^*(\xi, \eta) + U_{\text{sig}}^*(\xi, \eta)U_{\text{ref}}(\xi, \eta) \right] t_A(\xi, \eta). \quad (9)$$

Here, the second term of Equation (9) is a term that contributes to the conjugate image of the reconstructed image to be obtained, and originally corresponds to unnecessary interference fringes, but it is left to make the phase profile a real number.

### 3.3. Derivation of Diffracted Light in the Proposed Method

In order to understand the characteristics of diffracted light more clearly, we formulated the diffracted light  $U_{\text{dif}}(-x, -y)$  at the reconstructed image plane by assuming that the signal light and the reference light were discrete point groups;

$$\begin{cases} U_{\text{sig}}(x, y) = \Delta S \sum_{s=1}^{n_s} A_s e^{i\phi_s} \delta(x - x_s) \delta(y - y_s) \\ U_{\text{ref}}(x, y) = \Delta S \sum_{r=1}^{n_r} A_r e^{i\phi_r} \delta(x - x_r) \delta(y - y_r) \end{cases}, \quad (10)$$

where  $\Delta S$  represents a minute area of a signal light point and a reference light point,  $n_s$  and  $n_r$  represent the total number of the signal light points and reference light points respectively,  $A_s$  and  $A_r$  represent the amplitude at the coordinates  $(x_s, y_s)$  and  $(x_r, y_r)$  respectively, and  $\phi_s$  and  $\phi_r$  represent the phase at coordinates  $(x_s, y_s)$  and  $(x_r, y_r)$  respectively. In addition,  $\delta$  represents a delta function. Then, when Equation (9) is calculated by substituting Equation (10) into Equation (6), the obtained phase profile  $H'_p(\xi, \eta)$  is expressed as

$$\begin{aligned}
 H'_p(\xi, \eta) &= C'_p \left\{ \mathcal{F} [U_{\text{sig}}(x, y)] (\mathcal{F} [U_{\text{ref}}(x, y)])^* + (\mathcal{F} [U_{\text{sig}}(x, y)])^* \mathcal{F} [U_{\text{ref}}(x, y)] \right\} t_A(\xi, \eta) \\
 &= 2C'_p \left| \mathcal{F} [U_{\text{sig}}(x, y)] (\mathcal{F} [U_{\text{ref}}(x, y)])^* \right| \cos \left[ \arg \left\{ \mathcal{F} [U_{\text{sig}}(x, y)] (\mathcal{F} [U_{\text{ref}}(x, y)])^* \right\} \right] t_A(\xi, \eta) \\
 &= 2C'_p \left| \frac{\Delta S^2}{\lambda^2 f^2} \sum_{s=1}^{n_s} \sum_{r=1}^{n_r} A_s A_r e^{i(\phi_s - \phi_r)} e^{-i \frac{2\pi}{\lambda f} [(x_s - x_r)\xi + (y_s - y_r)\eta]} \right| t_A(\xi, \eta) \\
 &\quad \times \cos \left\{ \arg \left[ \frac{\Delta S^2}{\lambda^2 f^2} \sum_{s=1}^{n_s} \sum_{r=1}^{n_r} A_s A_r e^{i(\phi_s - \phi_r)} e^{-i \frac{2\pi}{\lambda f} [(x_s - x_r)\xi + (y_s - y_r)\eta]} \right] \right\}
 \end{aligned} \tag{11}$$

Here, "arg" represents the argument of a complex number. At this time, the exponential term  $\exp[iH'_p(\xi - \Delta\xi, \eta - \Delta\eta)]$  appearing in Equation (4) can be expressed as

$$\begin{aligned}
 e^{iH'_p(\xi - \Delta\xi, \eta - \Delta\eta)} &= \exp \left\{ i2C'_p \left| \frac{\Delta S^2}{\lambda^2 f^2} U_{s-r}(\xi, \eta) \right| t_A(\xi - \Delta\xi, \eta - \Delta\eta) \cos \left[ \arg \left( \frac{\Delta S^2}{\lambda^2 f^2} U_{s-r}(\xi, \eta) \right) \right] \right\} \\
 &= \sum_{N=-\infty}^{\infty} J_N \left( 2C'_p \left| \frac{\Delta S^2}{\lambda^2 f^2} U_{s-r}(\xi, \eta) \right| t_A(\xi - \Delta\xi, \eta - \Delta\eta) \right) i^N e^{iN \arg \left( \frac{\Delta S^2}{\lambda^2 f^2} U_{s-r}(\xi, \eta) \right)} \\
 &= \sum_{N=-\infty}^{\infty} J_N \left( 2C'_p \left| \frac{\Delta S^2}{\lambda^2 f^2} U_{s-r}(\xi, \eta) \right| t_A(\xi - \Delta\xi, \eta - \Delta\eta) \right) \left[ i \frac{U_{s-r}(\xi, \eta)}{|U_{s-r}(\xi, \eta)|} \right]^N,
 \end{aligned} \tag{12}$$

where  $J_N$  represents an  $N$ th-order Bessel function of the first kind, and  $U_{s-r}(\xi, \eta)$  is expressed as

$$U_{s-r}(\xi, \eta) = \sum_{s=1}^{n_s} \sum_{r=1}^{n_r} A_s A_r e^{i(\phi_s - \phi_r)} e^{-i \frac{2\pi}{\lambda f} [(x_s - x_r)\xi + (y_s - y_r)\eta]} e^{i \frac{2\pi}{\lambda f} [(x_s - x_r)\Delta\xi + (y_s - y_r)\Delta\eta]}. \tag{13}$$

Then, from the first equation to the second equation in Equation (12), the following equation is used;

$$e^{i\delta \cos \theta} = \sum_{N=-\infty}^{\infty} J_N(\delta) i^N e^{iN\theta}. \tag{14}$$

In addition, from the second equation to the third equation, the following equation is used;

$$e^{i \arg(z)} = \frac{z}{|z|}. \tag{15}$$

Therefore, when Equation (5) is calculated by substituting Equation (12) and Equation (13) into Equation (4), diffracted light on the reconstructed image plane  $U_{\text{dif}}(-x, -y)$  is expressed as

$$\begin{aligned}
 U_{\text{dif}}(-x, -y) &= \frac{\Delta S}{\lambda^2 f^2} \sum_{N=-\infty}^{\infty} \sum_{r'=1}^{n_r} \iint_{-\infty}^{\infty} t_A(\xi, \eta) A_{r'} J_N \left[ \frac{C_p \Delta S^2}{\lambda^2 f^2} |U_{s-r}(\xi, \eta)| t_A(\xi - \Delta\xi, \eta - \Delta\eta) \right] \\
 &\quad \times e^{i\phi_{r'}} \left[ i \frac{U_{s-r}(\xi, \eta)}{|U_{s-r}(\xi, \eta)|} \right]^N e^{i \frac{2\pi}{\lambda f} [(x - x_{r'})\xi + (y - y_{r'})\eta]} d\xi d\eta
 \end{aligned} \tag{16}$$

Here, the complex amplitude of the summation for  $N$  in Equation (16) represents the  $N$ th-order diffracted light contributing to the coordinates  $(u, v)$  of the reconstructed image plane, and it means that the final  $U_{\text{dif}}(-x, -y)$  is obtained by the coherent summation of the diffracted light of all diffraction orders.

#### 4. Simulation Condition and Result

In this research, a numerical simulation was conducted to investigate the signal to noise ratio (SNR) of the reconstructed image, shift selectivity, and effects of inter-page crosstalk due to multiple recording. The simulations were all performed by the numerical calculation software MATLAB.

It was necessary to convert the phase profile obtained by the theoretical formula into a discrete system and redesign it to a precision that could be realized by existing technology in order to conduct experiments. However, the influence of these methods of redesigning and considerations on the reconstructed images could not be explained at this stage. Since, this paper focused not on them but on explaining the novel and interesting features of a surface holographic memory, its theoretical description, and results of numerical simulations, the experimental methods and results will be future research subjects.

##### 4.1. Simulation Condition in Hologram Design

In this research, the original pattern images of the signal and reference light were used as shown in Figure 2. The calculation area was  $500 \times 500$  pixels and the pixel pitch was  $20 \mu\text{m}$ . The amplitudes of each signal light pixel and each reference light pixel were the same (the value was 1 in this numerical simulation) and the phase distribution was random. When conducting a readout experiment, these conditions could be satisfied using an intensity modulation type SLM in combination with a random phase mask.

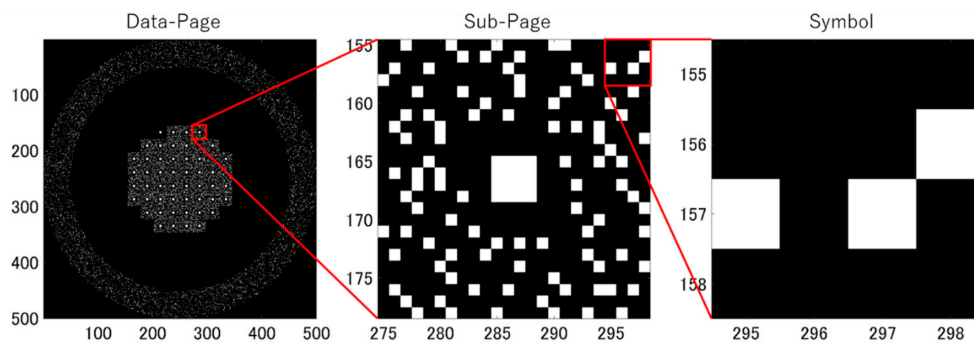


Figure 2. Original intensity pattern of signal pixels and reference pixels.

Then, a recording pattern called 3:16 modulation coding [9], which is generally used in holographic memory, was used as the signal pattern, and 51 subpages in one data page were arranged as shown in Figure 2. In this coding scheme, one subpage was composed of 32 symbols and one sync mark at the center for alignment. Then, one symbol was composed of  $4 \times 4$  pixels, of which only three pixels were ON pixels, and arranged without being adjacent to each other. Depending on the number of combinations of the three ON pixels, the data capacity of one byte per symbol was obtained, and as a result, the entire data page had a data capacity of 1632 bytes.

In addition, the width of each pixel of the SLM  $w_{\text{SLM}}$  was  $20 \mu\text{m}$ , the focal length of the lens  $f$  was 4 mm, and the wavelength of the light source  $\lambda$  was 405 nm. Here, the spatial spread width of the main lobe of the intensity distribution on the hologram plane (width between adjacent portions where the intensity is zero)  $D_{\text{Holo}}$  was represented as

$$D_{\text{Holo}} = \frac{\lambda f}{w_{\text{SLM}}} = 162 [\mu\text{m}]. \quad (17)$$

In this research, the aperture of the transmittance distribution  $t_A(\xi, \eta)$  expressed by Equation (3) was calculated as a rectangular aperture size of  $81 \mu\text{m} \times 81 \mu\text{m}$ , which was the smallest size satisfying the sampling theory. The reason the shape of the aperture was rectangular was that each pixel of the actual SLM was rectangular in this simulation.

#### 4.2. Signal to Noise Ratio (SNR) of Reconstructed Image

In this research, the SNR, defined by following Equation (18) [10], was used for the optimization of the phase coefficient:

$$\text{SNR} \equiv 20 \log_{10} \frac{|\mu_{\text{ON}} - \mu_{\text{OFF}}|}{\sigma_{\text{ON}} + \sigma_{\text{OFF}}} \text{ [dB]}, \tag{18}$$

where,  $\mu_{\text{ON}}$  or  $\mu_{\text{OFF}}$  represents the average intensity of the area within the reconstructed image that was ON pixel or OFF pixel respectively in the original signal pattern, and  $\sigma_{\text{ON}}$  and  $\sigma_{\text{OFF}}$  represents the standard deviation of the each area. A phase profile of a phase-only hologram used in this research was obtained by multiplying interference intensity distribution by the optimal phase coefficient. The phase coefficient was determined such that the SNR of the reconstructed image defined by Equation (18) was the highest.

#### 4.3. Reconstruction Property

First, the example of the signal area of the reproduced image in the surface holographic memory is shown in Figure 3. Here, Figure 3a shows the assumed original signal area pattern, and Figure 3b shows the signal area of the reconstructed image in the case that the unnecessary interference fringes were not included. These reconstructed images were assumed to be acquired by an image sensor, and the intensity level was corrected to 256 levels. As shown in Figure 3, we saw that the signal pattern in the collinear system was properly reconstructed even in a surface hologram whose thickness was substantially zero. Then, the effect of removing unnecessary interference fringes was evaluated. Histograms with and without the unnecessary interference fringes are shown in Figure 4a,b. The horizontal axis represents the intensity level, and the red and blue histograms respectively indicate the intensity distribution for the area within the reconstructed image that was ON pixel or OFF pixel respectively in the original signal pattern, and the vertical axis represents the percentage of the frequency. It can be seen from Figure 4 that the reconstructed image, when the unnecessary interference fringes were removed, was clear enough to reconstruct the original signal (error free can be expected by using error correction methods).

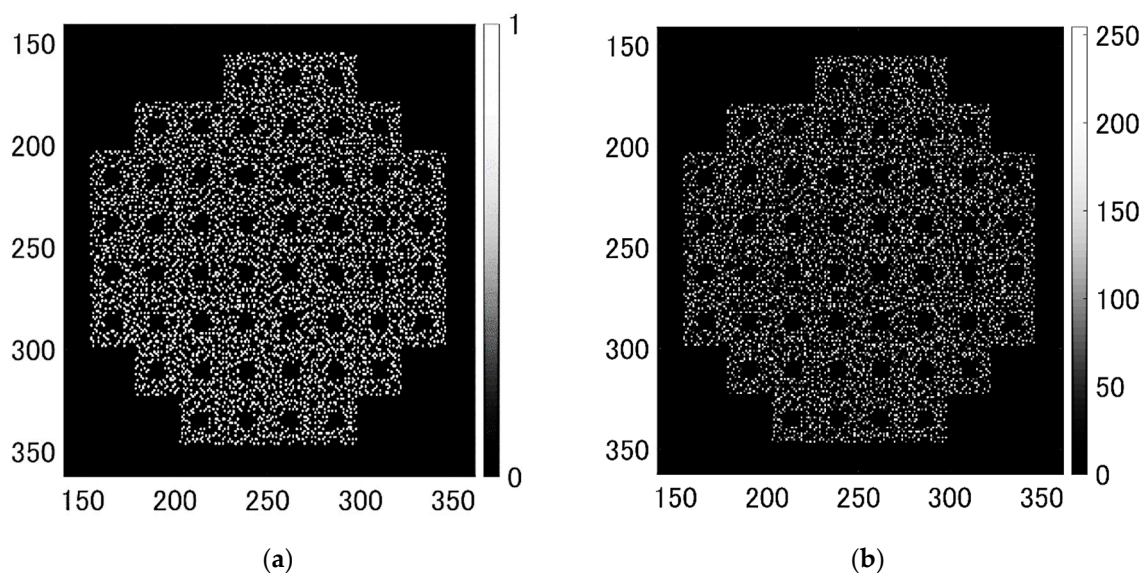


**Figure 3.** (a) Original pattern of signal area; (b) intensity distribution of reconstructed signal area. (omitting unnecessary interference).

From these histograms, it was estimated that the SNR in the case of including the unnecessary interference fringes was 3.8 dB and the SNR in the case of removing the unnecessary interference

fringes was 5.1 dB. From the results, it was confirmed that the SNR improved as expected when unnecessary interference fringes were removed.

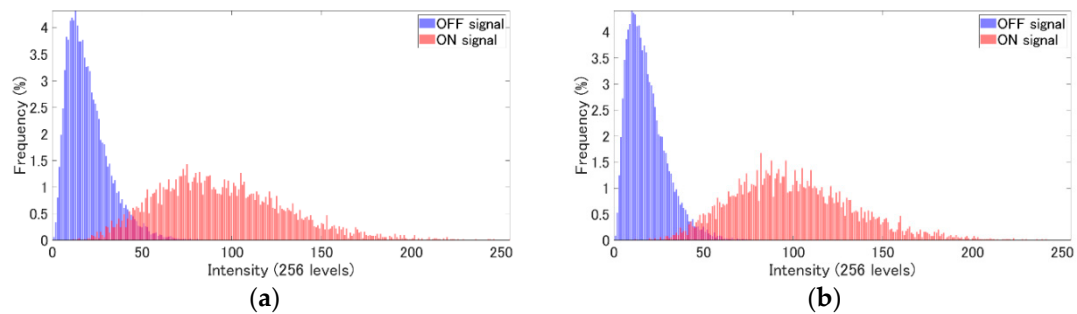


**Figure 4.** (a) Histogram of the reconstructed signal (including unnecessary interference), signal to noise ratio (SNR) = 3.8 dB; (b) histogram of the reconstructed signal (omitting unnecessary interference), SNR = 5.1 dB.

#### 4.4. Shift Selectivity

The relationship between the one-dimensional shift amount on the hologram plane and the diffraction efficiency in a hologram from which unnecessary interference fringes were removed is shown in Figure 5. Here, the diffraction efficiency was represented by the ratio of the sum of the intensities of the entire signal area to that of the whole reconstructed image plane. The horizontal axis represents the one-dimensional shift amount on the hologram plane, and the vertical axis represents the diffraction efficiency. From Figure 5, it is shown that the diffraction efficiency was maximized when the shift amount was zero, and it decreased significantly by a hologram shift of  $\pm 200$  nm. However, the diffraction efficiency did not decrease to a value close to zero, resulting in a bias of about 0.4%. A main reason of this is the high reconstruction tolerance of the surface hologram. Namely, random diffracted lights without information appeared though the image with information disappeared due to the shift selectivity.

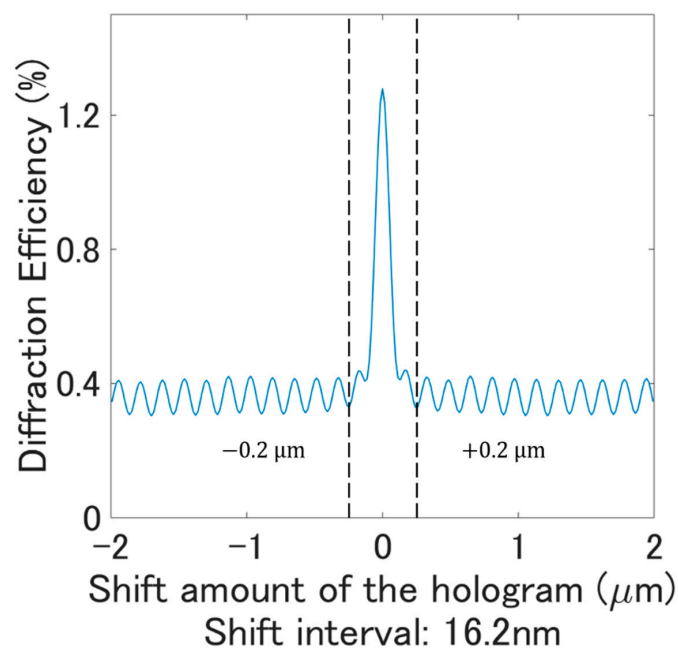


**Figure 5.** Shift selectivity of the surface collinear holographic memory.

#### 4.5. Influence of Inter-Page Crosstalk Due To Multiple Recording

According to the shift selectivity shown in Figure 5, although the diffraction efficiency of the signal decreased by the shift of the hologram a certain degree of bias remained. This meant that in the case of shift multiplexing, the influence from adjacent holograms (inter-page crosstalk) was stronger than that of the conventional collinear method. Therefore, the influence of this inter-page crosstalk was verified by numerical simulation. In this section, a total of nine multiplex holograms were considered, in which different holograms of  $81 \mu\text{m} \times 81 \mu\text{m}$  were overlapped and shifted by  $40.5 \mu\text{m}$  in eight vertical and horizontal directions. Moreover, unnecessary interference fringes were removed from all the holograms, and the  $81 \mu\text{m} \times 81 \mu\text{m}$  size hologram located at the center used the same hologram as in the case of Figure 5b. Therefore, in the hologram located at the center, the entire  $81 \mu\text{m} \times 81 \mu\text{m}$  area was totally multiplexed with other holograms. The histogram of the signal image reconstructed from the hologram located at the center overlapping other holograms is shown in Figure 6. As a result, the SNR was estimated to be  $-0.9 \text{ dB}$ , and it was shown that the SNR was greatly reduced from  $5.1 \text{ dB}$  to  $-0.9 \text{ dB}$  in only three multiplexes, compared with the case of the single hologram shown in Figure 4. Therefore, it has been confirmed that surface holographic memory is greatly affected by inter-page crosstalk.

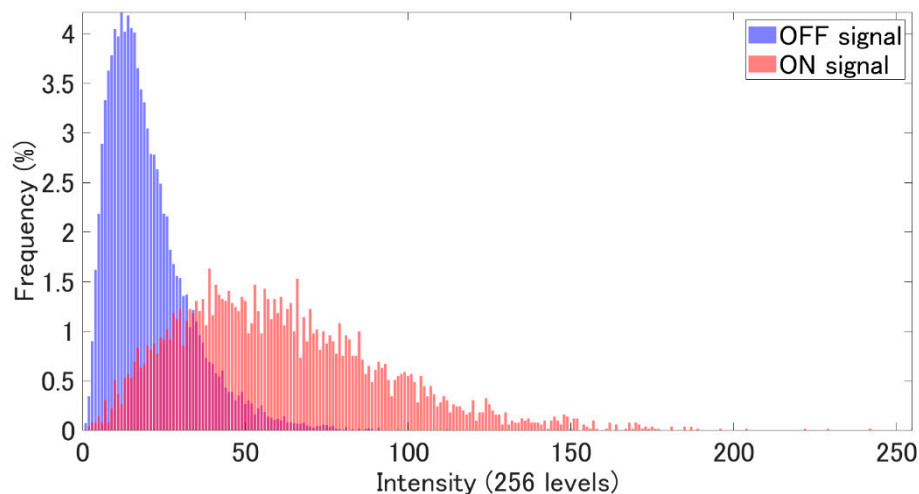


**Figure 6.** Histogram of the reconstructed signal area in case of three multiplexed hologram, SNR =  $-0.9 \text{ dB}$ .

This result means that the surface collinear holographic memory in the proposed method is not very suitable for shift multiplexing. However, it is considered that the degradation of the reconstructed image due to the high reconstruction tolerance can be suppressed by reducing the number of recorded gratings, in other words the total number of signal pixels or reference pixels assumed in the recording process. In that case, it is considered necessary to verify the optimal conditions because as the number of signal pixels decreases, the recording capacity per single page decreases, and as the number of reference pixels decreases, the shift amount required to reduce the diffraction efficiency of the reproduced image increases.

Recording density is determined by the hologram multiplicity and the data capacity per data-page. However, study of the limit of hologram multiplicity and data capacity per data page in the proposed method will be future research subjects because this paper explored principle recording and reconstruction of the proposed method.

## 5. Noise Factor of Surface Collinear Holographic Memory

A physically significant difference between the proposed method and the conventional collinear holographic memory is that the thickness of the hologram is in principle zero because the phase profile

of the hologram is represented by the physical surface asperity. As shown in Figure 4b, when the surface hologram was adapted to the collinear holographic memory, the reconstructed image contained noise, though unnecessary interference fringes between the signal light and the reference light were removed. In this section, two possible factors related to this noise, the influence of higher-order diffracted light and the degeneracy of the grating, are discussed.

In principle, surface holograms without thickness are dominated by Raman–Nath diffraction rather than Bragg diffraction in conventional volume holograms. In fact, the complex amplitude distribution of the diffracted light in Equation (16) is represented by the sum of the diffracted lights of all the diffraction orders. Among these diffracted lights, contributing to signal reconstruction is only the +1st-order diffracted light, and other diffracted lights cause noise. Figure 7 shows each intensity distribution on the reconstructed image plane when only diffracted light corresponding to each diffraction order (−2nd-, −1st-, 0th-, +1st- and 2nd-orders) was separated and calculated from Equation (16). As shown in Figure 7, the higher the diffraction order, the smaller the relative intensity of diffracted light. Thus, it can be assumed that the intensity of ±2nd-order or more diffracted light was negligibly small compared to the required +1st-order diffracted light. Only the −1st-order diffracted light had an intensity that could affect the +1st-order diffracted light, and further covered the entire signal area. As a result, we considered the −1st-order diffracted light to be the cause of the majority of the dominant noise among other diffraction orders.

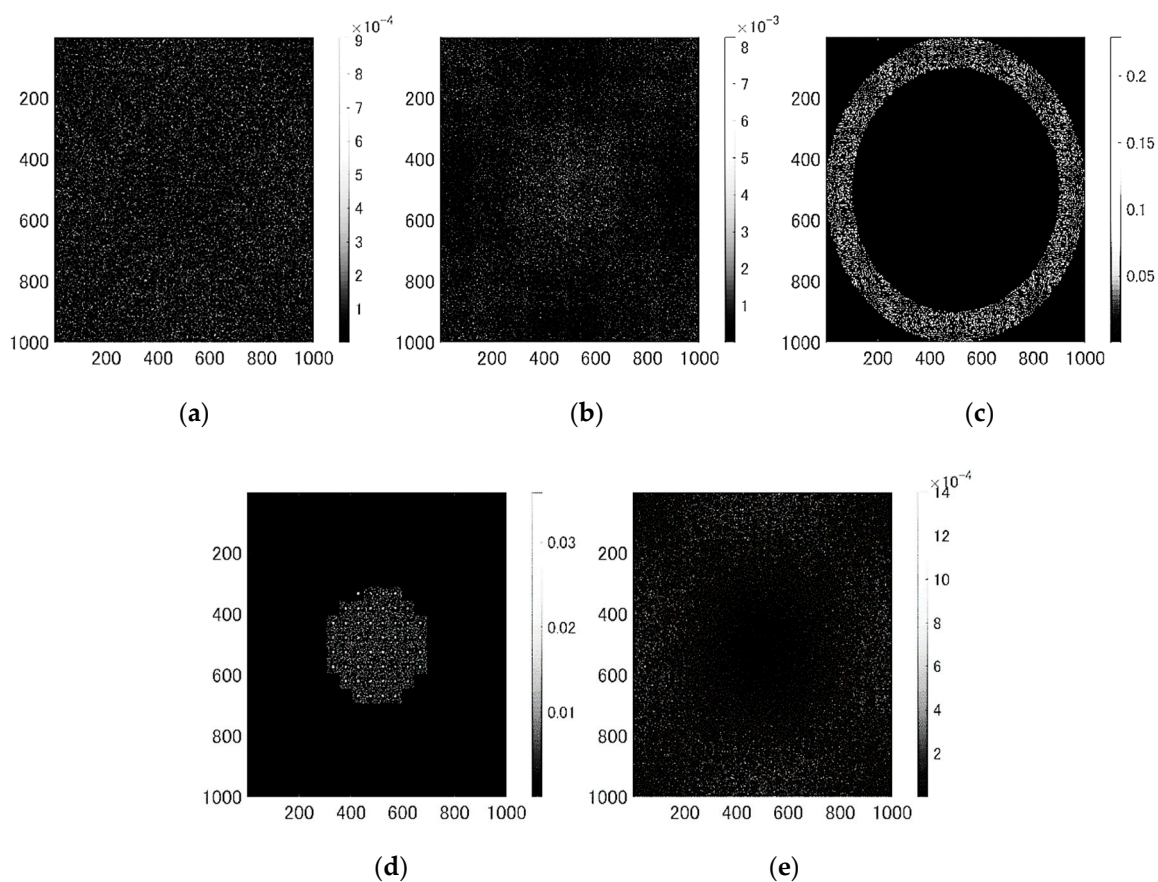


**Figure 7.** Each intensity distribution on the reconstructed image plane calculated by separating only each order diffracted light, (a) −2nd-order; (b) −1st-order; (c) 0th-order; (d) +1st-order; (e) +2nd-order.

Another possible cause of noise in the surface collinear holographic memory was the degeneracy of the grating. As an example, we assumed that two signal points  $S_1$  and  $S_2$  and two reference points  $R_1$  and  $R_2$  were arranged at different positions on the object plane at the time of recording. Under this condition, the propagated light from the reference point  $R_1$  at the time of reconstruction produced

diffracted light at the position  $S'_1$ , which is symmetrical to the point  $S_1$  at the time of recording with the diffracted light from the grating written by  $(S_1, R_1)$ . However, since the grating written by  $(S_2, R_2)$  was the same grating as  $(S_1, R_1)$ , diffracted light was similar at the position  $S'_1$ , which was the object of the optical axis with the point  $S_1$  at the time of recording. These diffracted lights arriving at the point  $S'_1$  interfered with each other due to the random phase pattern of the signal pixel and the reference pixel and, in many cases, the intensity of the area that should have been ON was reduced. In addition, the propagation light from the reference point  $R_1$  generated diffracted light by the grating from  $(S_1, R_2)$ , and also generated diffracted light in the area that should have been OFF in the original signal pattern. We considered the noise of diffracted light to be due to degeneration of these gratings, causing the SNR of the entire reproduced image to be lowered.

In this research, the arrangement of signal and reference patterns in a collinear system using shift multiplexing was adopted due to multiplex recording without using Bragg selectivity. However, according to the results of this research, inter-page crosstalk was much larger than the conventional method. Therefore, we assumed that the shift multiplex recording was not suitable as long as the collinear method was used. However, it was assumed that even surface holograms were not impossible to multiplex by properly setting the total number of signal pixels and reference pixels assumed at the time of recording to reduce the bias. This is because the intensity distribution of the bias spreads almost uniformly, though a certain bias remains when holograms shift. Furthermore, the surface holographic memory enabled not only collective duplication of page data by stamping and injection, which has been difficult in the case of volume holograms, but also stable readout by not using a photopolymer. Therefore, since surface holographic memory has many advantages, different from the conventional volume holographic memory, there is much value in research even if it is not well-suited to multiple recording.

## 6. Conclusions

The new type of holographic memory, a phase-only hologram represented by fine asperities of the surface, was proposed. This method enables collective duplication of page data by stamping and injection, which has been difficult in the case of conventional volume holograms while having the same high data transfer rate as conventional holographic memory. In addition, the storage stability of the recorded data is high because the recording material is not a photopolymer but a surface asperity structure. In this study, theoretical formulas of recording and reconstruction processes in the surface collinear holographic memory were derived. Furthermore, the noise of the reconstructed image was reduced compared to conventional optical writing methods recording unnecessary interference by designing a hologram from which unnecessary interference fringes were removed by using one of the unique features of the surface hologram.

However, in the reconstructed image noises that were not a problem in the conventional collinear method using volume holograms were generated. There are two possible causes of the noises. One is the influence of higher-order diffracted lights, and the other is the influence of degeneracy of the recorded gratings, and both of them are attributable to the fact that the thickness of the hologram was substantially zero. Although these noises deteriorated the SNR and shift selectivity of the reconstructed image, it was possible to reconstruct the signal image sufficiently in the case of a single page. This result shows the possibility of a new type of holographic memory.

In our research, arrangements of the signal and reference pattern in the collinear system are adopted in terms of multiple recording without using Bragg selectivity. As a result, we consider shift multiplex recording unsuited to the surface collinear system used in the proposed method. However, surface holographic memory has many advantages different from conventional volume holographic memory, and we consider it to have great research value.

Future work will examine new signal and reference patterns that are not bound to the collinear system in order to improve shift selectivity in surface holographic memory. Furthermore, in order to conduct experiments, we will study the optimal methods to convert the phase profile obtained

by the theoretical formula into a discrete system and redesign to a precision that can be realized by existing technology. A leading candidate we are currently focusing on for conducting the experiment is a hologram that will be represented by arranging metal pieces that are sufficiently smaller than the wavelength in order to use the interaction between light and plasmon.

**Author Contributions:** Conceptualization, S.H., R.F., S.U., and T.S.; methodology, S.H., R.F., and T.S.; writing—original draft preparation, S.H.; writing—review and editing, R.F., S.U., Y.Y.T., and T.S.; project administration, T.S.

**Funding:** This research received no external funding.

**Conflicts of Interest:** The funders had no role in the design of the study, collection, analyses or interpretation of data, in the writing of the manuscript, or in the decision to publish the results.

## References

1. Leith, E.N.; Kozma, A.; Upatnieks, J.; Marks, J.; Massey, N. Holographic data storage in three-dimensional media. *Appl. Opt.* **1966**, *5*, 1303–1311. [[CrossRef](#)] [[PubMed](#)]
2. Mok, F.H. Angle-multiplexed storage of 5000 holograms in lithium niobate. *Opt. Lett.* **1993**, *18*, 915–917. [[CrossRef](#)] [[PubMed](#)]
3. Glezer, E.N.; Milosavljevic, M.; Huang, L.; Finlay, R.J.; Her, T.H.; Callan, J.P.; Mazur, E. Three-dimensional optical storage inside transparent materials. *Opt. Lett.* **1996**, *21*, 2023–2025. [[CrossRef](#)] [[PubMed](#)]
4. Van Heerden, P.J. Theory of optical information storage in solids. *Appl. Opt.* **1963**, *2*, 393–400. [[CrossRef](#)]
5. Gabor, D. A new microscopic principle. *Nature* **1948**, *161*, 777–778. [[CrossRef](#)] [[PubMed](#)]
6. Horimai, H.; Tan, X.; Li, J. Collinear holography. *Appl. Opt.* **2005**, *44*, 2575–2579. [[CrossRef](#)] [[PubMed](#)]
7. Shoydin, S.A. Holographic memory without reference beam. *Opt. Mem. Neural Netw.* **2016**, *25*, 262–267. [[CrossRef](#)]
8. Psaltis, D.; Levene, M.; Pu, A.; Barbastathis, G.; Curtis, K. Holographic storage using shift multiplexing. *Opt. Lett.* **1995**, *20*, 782–784. [[CrossRef](#)] [[PubMed](#)]
9. King, B.M.; Neifeld, M.A. Sparse modulation coding for increased capacity in volume holographic storage. *Appl. Opt.* **2000**, *39*, 6681–6688. [[CrossRef](#)] [[PubMed](#)]
10. Curtis, K.; Dhar, L.; Hill, A.; Wilson, W.; Ayres, M. *Holographic Data Storage: From Theory to Practical Systems*, 1st ed.; John Wiley and Sons Ltd.: Hoboken, NJ, USA, 2010; pp. 253–254.



© 2019 by the authors. Licensee MDPI, Basel, Switzerland. This article is an open access article distributed under the terms and conditions of the Creative Commons Attribution (CC BY) license (<http://creativecommons.org/licenses/by/4.0/>).